Biologically Inspired Planning and Optimization of Foot Trajectory of a Quadruped Robot

Senwei Huang and Xiuli Zhang(✉)

School of Mechanical, Electronic and Control Engineering,
Beijing Jiaotong University, Beijing 100044, China
zhangxl@bjtu.edu.cn

Abstract. Foot trajectory plays an important role in high speed running of cheetahs, so it is very significant to design an appropriate foot trajectory by mimicking cheetahs to improve the performance of quadruped robots. This paper presents a Bézier curve based foot trajectory planning approach for a quadruped robot. Four 5th-order Bézier curves are employed to plan the robot's foot trajectory in the sagittal plane, which is inspired by the foot trajectory characteristics of cheetahs. Particle swarm optimization algorithm is used to determine the foot trajectory parameters with the aim of minimizing the jerk of the trajectory and impact as the feet touch the ground. Finally, the joints trajectories are computed through the inverse kinematic of the quadruped robot. Moreover, the foot trajectory is parametrized for applying to robots with different sizes. The dynamic simulation results show that the generated foot trajectory is effective to approximately achieve the desired speeds.

Keywords: Foot trajectory planning · Bio-inspired · Particle swarm optimization · Bézier curve · Quadruped robot

1 Introduction

In recent years, quadruped robot develops rapidly and has shown great control performance [1–5]. Foot trajectory plays an important role in the motion performance of the quadruped robot because the foot trajectory determines the interaction between the foot and the ground. An inappropriate foot trajectory will lead to bad impact force, which will greatly influence the continuity, stability, and efficiency of the quadruped robot. As a solution to this problem, many kinds of foot trajectory planning methods were proposed, such as rectangular foot trajectory [6], elliptical foot trajectory [7], composite cycloid foot trajectory [8], composite foot trajectory [9], polynomial foot trajectory [10], and Bézier foot trajectory [11].

X.-J. Liu et al. (Eds.): ICIRA 2021, LNAI 13016, pp. 192–203, 2021.
https://doi.org/10.1007/978-3-030-89092-6_18

The composite cycloid foot trajectory which was proposed by Sakakibara et al. [7] takes the step length, height, and step phase times as parameters. HyQ [12] achieves approximately a 2 m/s trot by applying the composite cycloid foot trajectory. Scalf-1 [13] robot uses composite cycloid foot trajectory to avoid foot-dragging when walking. Wang et al. [14] modified the method of composite cycloid to plan the foot trajectory with zero impact. Yin et al. [15] use a composite cycloid to plan the foot trajectory and realize the tracking of the foot trajectory by combining neural networks and reinforcement learning methods. The Bézier foot trajectory is widely used for its advantages over the past few years. The foot trajectories of Cheetah-Cub [16] were generated by four quadratic Bézier curves. The stability of the Cheetah-Cub is improved by adjusting the leg angle at the moment of take-off and touch-down. Serval [17] achieves many motion patterns, simply by replaying parameterized foot trajectory which is generated by fitting four cubic Bézier curves to the foot trajectory data of dog. MIT Cheetah2 [18] robot's foot trajectory of swing phase is based on three 5th-order Bézier curves. Han et al. [19] used an 11th order Bézier curve to plan the foot trajectory of a quadruped robot and improved the walking stability by optimizing the step height and step length.

Various foot trajectories have been developed and studied to improve the locomotion performance of the quadruped robot. However, there is still a lot of work that has to be done in the field of quadruped robot trajectory planning. This paper deals with the foot trajectory design for a quadruped robot. We propose here an approach: we define in the sagittal plane our desired foot trajectory, we parameterize trajectory that is close to the cheetah, and the joints trajectory are computed through the inverse kinematic. Instead of designing a fixed trajectory, we aim to parameterize it with variables that are meaningful for locomotion.

The following section introduces the quadruped robot model. Section 3 introduces foot trajectory planning and optimization based on Bézier curve and particle swarm optimization. Section 4 verifies the effectiveness of the foot trajectory in simulation, and Sect. 5 concludes the paper and discusses future work.

2 Quadruped Robot

By mimicking quadruped mammals, we constructed a quadruped robot model in the Adams simulation environment. As shown in Fig. 1, the robot has a trunk and four legs. Each leg includes a femur, a tibia, and a foot. The hip and knee joints have one active pitch degree of freedom respectively. The foot is fixed at the lower end of the tibia. The material of the foot is defined as rubber, which reduces impact and increases friction. The main mechanical parameters of the quadruped robot are given in Table 1. The robot has dimensions of 1.05 m $\times$ 0.56 m $\times$ 0.7 m, and a mass of 23.85 kg. The following sections introduce the foot trajectory planning and optimization of the quadruped robot.

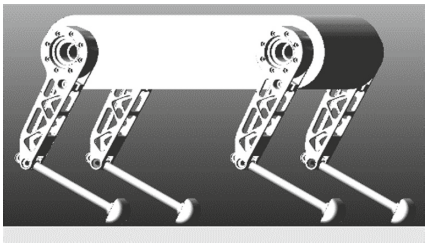

Fig. 1. 3D model of the quadruped robot

Table 1. Mechanical parameters of the quadruped robot

Link	Length (m)	Mass (kg)	Inertia ($kg \cdot m^2$)
Trunk	0.8	10	0.534
Femur	0.4	2	0.006
Tibia	0.34	0.2	0.00002
Foot	0.046	0.0001	/

3 Planning and Optimization of the Foot Trajectory

3.1 Biological Observation and Analysis

The paths followed by the feet and leg joints of a cheetah in relation to fixed points at the shoulder and the hip were depicted by Hildebrand [20, 21]. Figure 2 shows the hindfoot and joints trajectories of a cheetah. There is a retraction segment in the foot trajectory before the foot touches the ground. After the foot leaves the ground, there is a backswing segment, which is symmetrical with the retraction segment. In this paper, the foot trajectory is divided into one stance phase (ST) and one swing phase (SW) with reference to [18]. The swing phase is divided into three sub-phases, namely, a follow-through (FT), a protraction (PR), and a swing-leg-retraction (SR), which happen in sequence. Four transitional points of the four phases are defined, as shown in Fig. 2(a).

To simplify the design and optimization process, each leg of the cheetah is treated as a virtual leg, which has only two important parameters: length (distance from foot to shoulder or hip) and angle (angle between the virtual leg and the horizontal plane). The posterior extension point (pep) means that the virtual leg has reached the maximum angle when swinging backward. The anterior extension point (aep) means that the virtual leg has reached the maximum angle when swinging forward. The data presented in [21] was used to analyze the foot trajectory characteristics of the cheetah through the kinematic method. The locomotion of the virtual leg at pep and aep has the following characteristics: (1) the angle reaches the maximum or minimum; (2) the angular velocity is close to 0; (3) the contraction speed of the virtual leg is close to the maximum. Take-off is where the foot begins to leave the ground. Touch-down is where the foot begins to touch the ground. The locomotion of the virtual leg at take-off and touch-down has the following characteristics: (1) the length reaches the maximum; (2) the contraction speed is close to 0.

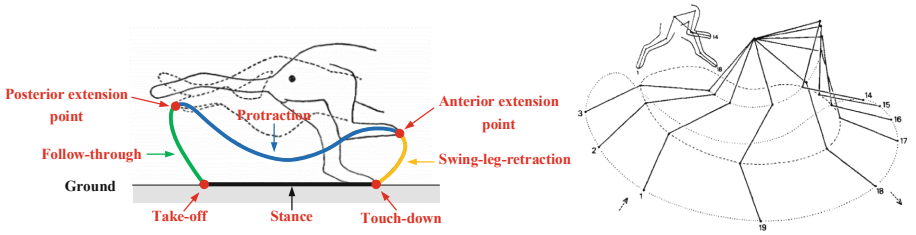

Fig. 2. (a) Hindfoot trajectory in the sagittal plane of a cheetah galloping at 50 to 60 mph. The foot trajectory is divided into FT, PR, SR, and ST phases, which are represented by green, blue, yellow, and black lines, respectively. (b) Joint angles and successive positions of hindlimb segments of a cheetah galloping at roughly 56 mph. Arrows show the approximate times of take-off and touch-down. (Color figure online)

3.2 Foot Trajectory Planning Based on Bézier Curves

The desired foot trajectory can be generated and parameterized using the Bézier curve. The points that are used to define a Bézier curve are called control points. A Bézier curve of degree n can be represented as

$$C(u) = \sum_{i=0}^{n} B_{n,i}(u) P_i \tag{1}$$

where $B_{n,i}(u)$ is a Bernstein Polynomial given by $B_{n,i}(u) = \frac{n!}{i!(n-i)!} u^i (1-u)^{n-i}, u \in [0, 1]$ is a parameter of the Bézier curve, and P_i are the Bézier curve control points.

To plan the time of each phase of the foot trajectory, time coefficient a is introduced to map phase duration t into the parameter of the Bézier curve u, as shown in Eq. (2).

$$u = at, \quad t \in [0, t_{\max}] \tag{2}$$

where a is the time coefficient given by $a = 1/t_{\max}$. $t_{\max}$ is phase duration required for the foot to move from the first to the last point of the Bézier curve.

The first derivative of a Bézier curve of degree n is a Bézier curve of degree $n-1$,

$$C'(at) = \sum_{i=0}^{n-1} B_{n-1,i}(at)\left[na(P_{i+1} - P_i)\right] \tag{3}$$

It is easy to obtain $C(0) = P_0$ and $C'(0) = na(P_1 - P_0)$ at $t = 0$, $C(1) = P_n$ and $C'(1) = na(P_n - P_{n-1})$ at $t = t_{\max}$. The first and last points on the curve are coincident with the first and last control points. The speed of the start (end) of a Bézier curve can be controlled by the position of the first (last) two control points and time coefficient.

A foot trajectory is generated by connecting four 5th-order Bézier curves. We plan the foot trajectory in the polar coordinate system and take the center of the hip joint as the origin. The coordinates of the control points of the foot trajectory are defined as,

$$P_i^j = [\phi_i^j, l_i^j]^T, \quad i \in \{0, 1, \cdots, 5\}, \quad j \in \{\text{FT,PR,SR,ST}\} \tag{4}$$

Here, P_i^j represent the coordinate of the ith control point of the jth segment of the foot trajectory, ϕ_i^j and l_i^j is the polar angle and diameter of the control point. Subscripts $i \in \{0, 1, \cdots, 5\}$ and $j \in \{\text{FT,PR,SR,ST}\}$ indicate control point and phase index.

3.3 Definition of Constraints and Optimization Variables

The connecting points of the foot trajectory are selected in order to provide continuous and smooth transitions by subject to the following constraints

$$P_5^{\text{FT}} = P_0^{\text{PR}},\ P_5^{\text{PR}} = P_0^{\text{SR}},\ P_5^{\text{SR}} = P_0^{\text{ST}},\ \text{and}\ P_5^{\text{ST}} = P_0^{\text{FT}} \tag{5}$$

$$\begin{aligned} a_{\text{FT}}(P_5^{\text{FT}} - P_4^{\text{FT}}) = a_{\text{PR}}(P_1^{\text{PR}} - P_0^{\text{PR}}),\quad a_{\text{PR}}(P_5^{\text{PR}} - P_4^{\text{PR}}) &= a_{\text{SR}}(P_1^{\text{SR}} - P_0^{\text{SR}}) \\ a_{\text{SR}}(P_5^{\text{SR}} - P_4^{\text{SR}}) = a_{\text{ST}}(P_1^{\text{ST}} - P_0^{\text{ST}}),\quad a_{\text{ST}}(P_5^{\text{ST}} - P_4^{\text{ST}}) &= a_{\text{FT}}(P_1^{\text{FT}} - P_0^{\text{FT}}) \end{aligned} \tag{6}$$

Combining Eq. (5) and (6) yields

$$P_1^{\text{PR}} = P_5^{\text{FT}} + \frac{a_{\text{FT}}}{a_{\text{PR}}}\left(P_5^{\text{FT}} - P_4^{\text{FT}}\right),\quad P_4^{\text{PR}} = P_0^{\text{SR}} + \frac{a_{\text{SR}}}{a_{\text{PR}}}\left(P_0^{\text{SR}} - P_1^{\text{SR}}\right) \tag{7}$$

$$P_1^{\text{ST}} = P_5^{\text{SR}} + \frac{a_{\text{SR}}}{a_{\text{ST}}}\left(P_5^{\text{SR}} - P_4^{\text{SR}}\right),\quad P_4^{\text{ST}} = P_0^{\text{FT}} + \frac{a_{\text{FT}}}{a_{\text{ST}}}\left(P_0^{\text{FT}} - P_1^{\text{FT}}\right) \tag{8}$$

According to the conclusion that the angular velocity of the virtual leg at pep and aep is close to 0 ($\dot{\phi}_0^{\text{FT}} = \dot{\phi}_5^{\text{SR}} = 0$). We obtain the following constraints

$$\phi_4^{\text{FT}} = \phi_5^{\text{FT}} = \phi_0^{\text{PR}} = \phi_1^{\text{PR}},\ \phi_4^{\text{PR}} = \phi_5^{\text{PR}} = \phi_0^{\text{SR}} = \phi_1^{\text{SR}} \tag{9}$$

According to the conclusion that the contraction speed of the virtual leg at take-off and touch-down is close to 0 ($\dot{l}_0^{\text{FT}} = \dot{l}_5^{\text{SR}} = 0$). We obtain the following constraints

$$l_0^{\text{FT}} = l_1^{\text{FT}} = l_4^{\text{ST}} = l_5^{\text{ST}},\quad l_0^{\text{ST}} = l_1^{\text{ST}} = l_4^{\text{SR}} = l_5^{\text{SR}} \tag{10}$$

The step length (L) and hip height (H) is introduced into the foot trajectory planning, see Fig. 3. Virtual leg angle and length at take-off and touch-down can be obtained by

$$\begin{aligned} \phi_0^{\text{FT}} &= \pi + \arctan(2H/L) \\ l_0^{\text{FT}} &= -\text{H}/\sin(\phi_0^{\text{FT}}) \end{aligned} \tag{11}$$

$$\begin{aligned} \phi_5^{\text{SR}} &= 2\pi - \arctan(2H/L) \\ l_5^{\text{SR}} &= -\text{H}/\sin(\phi_5^{\text{SR}}) \end{aligned} \tag{12}$$

The research of Haberland et al. [22], Karssen et al. [23], and Park et al. [18] show that the relative speed of the foot with respect to the ground at the moment of touchdown can be reduced by retracting the swing leg. And the reduced foot speed can help reduce impact energy losses, decrease peak forces, and minimize foot slipping, as well as improve the stability and disturbance rejection of running robots. The optimal retraction rate,

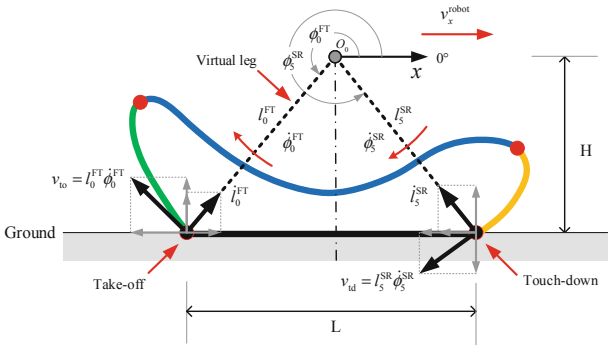

Fig. 3. Design of foot trajectory in the polar coordinate system with the origin (O_0) at the hip.

for which the impact force and impact losses are minimal, is the retraction at which the tangential foot speed (magnitude of the velocity of the foot in the direction perpendicular to the leg) is zero. According to this conclusion, the swing leg retraction rate $\dot{\phi}_5^{\mathrm{SR}}$ will be calculated to satisfy $\dot{\phi}_5^{\mathrm{SR}} l_5^{\mathrm{SR}} - v_x^{\mathrm{robot}} \sin(\phi_5^{\mathrm{SR}}) = 0$; therefore the following constraint equation can be derived,

$$5a_{\mathrm{SR}}(\phi_5^{\mathrm{SR}} - \phi_4^{\mathrm{SR}}) l_5^{\mathrm{SR}} - v_x^{\mathrm{robot}} \sin \phi_5^{\mathrm{SR}} = 0 \tag{13}$$

The horizontal velocity of the foot v_x^{robot} is equal to the horizontal velocity of the robot at the moment of take-off, expressed as $v_x^{\mathrm{robot}} - v_t^{\mathrm{to}} \sin \phi_0^{\mathrm{FT}} = 0$. The constraint equation can be expressed as

$$v_x^{\mathrm{robot}} - 5a_{\mathrm{FT}}(\phi_1^{\mathrm{FT}} - \phi_0^{\mathrm{FT}}) l_0^{\mathrm{FT}} \sin \phi_0^{\mathrm{FT}} = 0 \tag{14}$$

Therefore, the coordinates of the control points that are needed to generate a complete foot trajectory are defined by,

$$\begin{aligned}
P^{\mathrm{FT}} &= \begin{bmatrix} \phi_0^{\mathrm{FT}} & f_1 & x_1 & x_2 & x_3 & x_3 \\ l_0^{\mathrm{FT}} & l_0^{\mathrm{FT}} & x_{11} & x_{12} & x_{13} & x_{14} \end{bmatrix} \\
P^{\mathrm{PR}} &= \begin{bmatrix} x_3 & x_3 & x_4 & x_5 & x_6 & x_6 \\ x_{14} & f_2 & x_{15} & x_{16} & f_3 & x_{17} \end{bmatrix} \\
P^{\mathrm{SR}} &= \begin{bmatrix} x_6 & x_6 & x_7 & x_8 & f_4 & \phi_5^{\mathrm{SR}} \\ x_{17} & x_{18} & x_{19} & x_{20} & l_5^{\mathrm{SR}} & l_5^{\mathrm{SR}} \end{bmatrix} \\
P^{\mathrm{ST}} &= \begin{bmatrix} \phi_5^{\mathrm{SR}} & f_5 & x_9 & x_{10} & f_6 & \phi_0^{\mathrm{FT}} \\ l_5^{\mathrm{SR}} & l_5^{\mathrm{SR}} & x_{21} & x_{22} & l_0^{\mathrm{FT}} & l_0^{\mathrm{FT}} \end{bmatrix}
\end{aligned} \tag{15}$$

where x_i are the parameters to be determined by optimization. The coordinates of the take-off, $[\phi_0^{\mathrm{FT}}, l_0^{\mathrm{FT}}]^T$, and touch-down, $[\phi_5^{\mathrm{SR}}, l_5^{\mathrm{SR}}]^T$, can be calculated by Eq. (11) and (12). f_1 can be calculated by Eq. (13). f_2 and f_3 can be calculated by Eq. (7). f_4 can be calculated by Eq. (14). f_5 and f_6 can be calculated by Eq. (8).

The duration of the FT, PR, SR, and ST phases are defined by t_{FT}, t_{PR}, t_{SR}, and t_{ST}, respectively. The total duration is given by $T = t_{\mathrm{FT}} + t_{\mathrm{PR}} + t_{\mathrm{SR}} + t_{\mathrm{ST}}$. The ratio of the

duration of FT, PR, SR, and ST phases to the total duration is defined as x_{23}, x_{24}, and x_{25}, respectively. Therefore the following equation can be derived,

$$t_{\mathrm{FT}} = x_{23}T, \quad t_{SR} = x_{24}T, \quad t_{\mathrm{ST}} = x_{25}T, \quad \text{and } t_{PR} = (1 - x_{23} - x_{24} - x_{25})T \tag{16}$$

To sum up, only 25 parameters need to be determined to generate the desired foot trajectory. Vector $x \in R^{25}$, which parameterizes the desired foot trajectory, is defined as,

$$x = \begin{bmatrix} x_1 \; x_2 \; \cdots \; x_{25} \end{bmatrix} \tag{17}$$

The first 22 elements of x, $x_{1\cdots22}$, are used to parameterize the desired trajectory of the FT, PR, SR, and ST phases. The last three elements of x, $x_{23\cdots25}$ determine the durations of the FT, PR, and SR phases.

3.4 Parameter Optimization Based on Particle Swarm Optimization

This paper uses the particle swarm optimization (PSO) algorithm to determine these 25 parameters. PSO is a bionic optimization algorithm proposed by Kennedy and Eberhart [24]. Here, the position of each particle represents a foot trajectory, and the 25 dimensions of the particle represent 25 parameters that are used to determine a foot trajectory. The speed and position update methods are given by Eq. (18) and (19), respectively.

$$v_{id}^{k+1} = \omega v_{id}^{k} + c_1 r_1 \left(p_{id,\mathrm{pbest}}^{k} - x_{id}^{k} \right) + c_2 r_2 \left(p_{d,\mathrm{gbest}}^{k} - x_{id}^{k} \right) \tag{18}$$

$$x_{id}^{k+1} = x_{id}^{k} + v_{id}^{k+1} \tag{19}$$

Where $i = 1, 2, \cdots, N$ is particle number, N is particle swarm size. $d = 1, 2, \cdots, D$ is particle dimension number. k is iterations. ω is inertia weight. c_1 and c_2 are individual and group learning factors. r_1 and r_2 are random numbers in [0,1]. v_{id}^{k} and x_{id}^{k} are the velocity and position vector of the particle i in the k iteration. $p_{id,\mathrm{pbest}}^{k}$ and $p_{d,\mathrm{gbest}}^{k}$ are the historical optimal position of the individual and group in the k iteration.

Objective: Minimize norm of the jerk of the trajectory,

$$\sum^{j\in\{\mathrm{FT,PR,SR,ST}\}} \left\| \frac{d^3}{dt^3} \phi^j \right\| + \sum^{j\in\{\mathrm{FT,PR,SR,ST}\}} \left\| \frac{d^3}{dt^3} l^j \right\| \tag{20}$$

In order to generate an available foot trajectory for a quadruped robot, optimization should subject to constraints shown in Table 2. The initial conditions are shown in Table 3. We optimize three foot trajectories that have expected speeds of 1 m/s, 2 m/s, and 3 m/s respectively. After 100 iterations, the particle fitness value has reached a stable value. The foot trajectories are shown in Fig. 4.

Table 2. The constraints of the virtual leg

Parameters	Value range
Leg angle (rad)	3.752–5.498
Leg length (m)	0.363–0.785
Leg angular velocity (rad/s)	−25–25
Leg stretching speed (m/s)	−4–4

Table 3. Initial conditions

Parameters	Value
Total duration (s)	1, 0.75, and 0.6
Horizontal velocity (m/s)	1, 2, and 3
Hip height (m)	0.55
Step length (m)	0.4

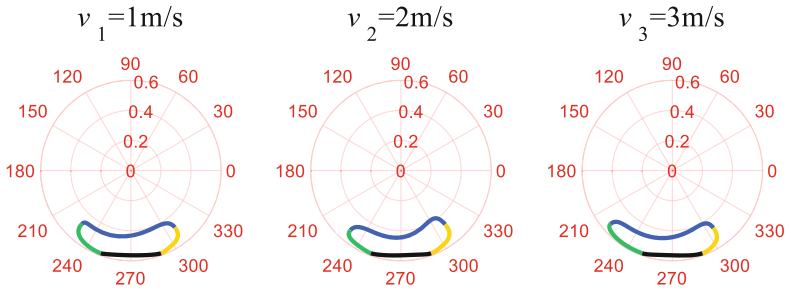

Fig. 4. The foot trajectories with expected speeds of 1 m/s, 2 m/s, and 3 m/s.

4 Simulations

In this section, the effectiveness of foot trajectories is verified in several simulation tests. We control the quadruped robot to gallop three times for 20 s in the Adams simulation environment with three types of foot trajectories, respectively. Figure 5 shows snapshots within one gait cycle when the quadruped robot gallops at 1 m/s. The video shows the robot can walk steadily when controlled by the designed joint trajectories.

The horizontal speeds of the center of mass (CoM) when using three foot trajectories respectively, see Fig. 6. The speed of CoM fluctuates periodically along with this robot's galloping locomotion. And the fluctuation of speed increases with the increase of speed. The first foot trajectory v_1 which desired speed is 1 m/s achieves an average speed of 1.287 m/s. The second foot trajectory v_2 which desired speed is 2 m/s achieves an average speed of 1.716 m/s. The third foot trajectory v_3 which desired speed is 3 m/s achieves an average speed of 2.239 m/s. The results show the desired speeds can be roughly achieved. But the differences between the actual speeds and the expected speeds are becoming greater as the running speed increases. This is mainly due to the inaccurate position control, which leads to the leg touching the ground at an unexpected joint position and speed. Besides, the ground reaction force (GRF) increases gradually as the running speed increase, as shown in Fig. 7. The increased impact forces cause unstable locomotion, which makes the desired velocity cannot be fully achieved. Since the robot does not have an elastic element, the GRF is fairly large. So we consider adding an elastic element to each leg in future work.

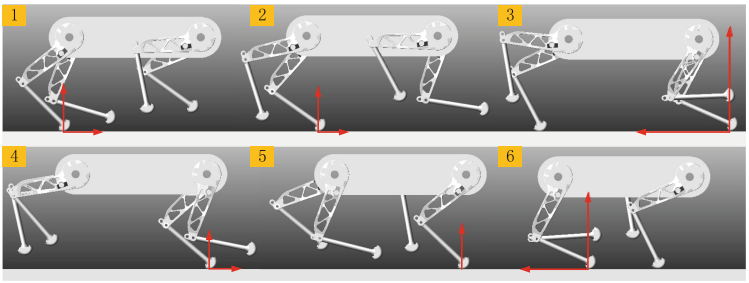

Fig. 5. Snapshots of the simulated quadruped robot galloping at 1 m/s. The red arrows represent the direction of GRF. (Color figure online)

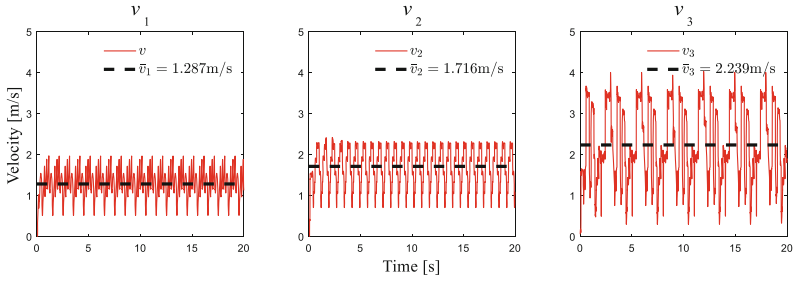

Fig. 6. The velocity of CoM of the simulated quadruped robot.

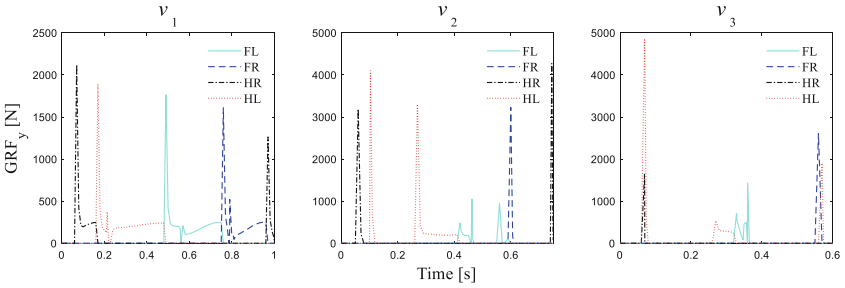

Fig. 7. Ground reaction forces in the vertical direction within one gait cycle. Solid cyan line, dashed blue line, dotted black line, and dash-dotted red line represents front left foot (FL), front right foot (FR), hind right foot (HR), and hind left foot (HL), respectively. (Color figure online)

Figure 8 and Fig. 9 show the front left leg joint torques within one gait cycle. The torque acting on each joint changes periodically and fluctuates while the phase of trajectory is changing. And the joint torque reaches the maximum when the foot is touching the ground or crossing the phase transition points of four phases. Because the acceleration at these positions changes dramatically, the jerk of the actuator will be very large. It is necessary to consider the change of acceleration at the phase transition point in future work when connecting multiple Bézier curves to generate foot trajectory. The

joint torque is smooth while the foot is in other positions of the foot trajectory, so the jerk of the actuator can be reduced.

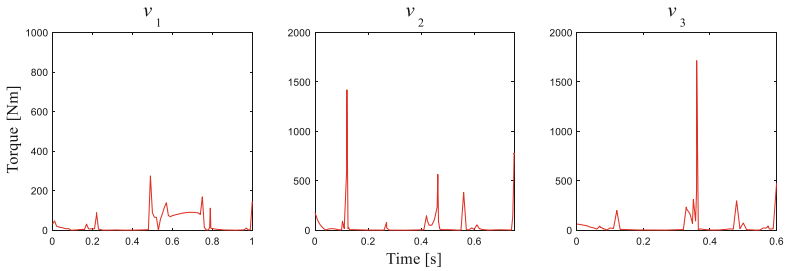

Fig. 8. The torque acting on the hip joint of front left leg.

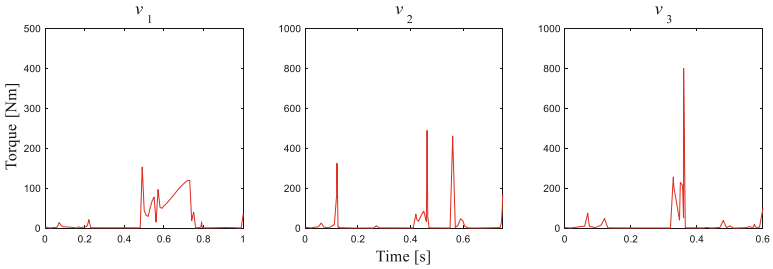

Fig. 9. The torque acting on the knee joint of front left leg.

5 Conclusions

We proposed a parameterized approach using hip height, step height, horizontal velocity of the robot, and step phase times for trajectory generation of a quadruped robot. The desired foot trajectories are planned using four 5th-order Bézier curves in which the control points are constrained by referring to the cheetah's biological data. Particle swarm optimization algorithm is applied to determine the foot trajectory parameter. The foot trajectories are effective and the desired speeds can be roughly achieved on a simulated quadruped robot. As the robot has no elastic component, the GRF is quite large. The joint torque is comparatively large when the foot is touching the ground or crossing the connection points of the Bézier curves. For the future work, we can improve the constraint conditions of trajectory planning when connecting multiple Bézier curves.

References

1. Yang, C., Yuan, K., Zhu, Q., Yu, W., Li, Z.: Multi-expert learning of adaptive legged locomotion. Sci. Robot. **5**(49), 1–14 (2020)
2. Shandong youbaote intelligent robotics co., ltd. http://www.yobotics.cn. Accessed 20 Apr 2021
3. WEILAN. http://www.weilan.com. Accessed 20 Apr 2021
4. Bledt, G., Kim, S.: Extracting legged locomotion heuristics with regularized predictive control. In: IEEE International Conference on Robotics and Automation, pp. 406–412. IEEE Press, Paris (2020)
5. Lee, J., Hwangbo, J., Wellhausen, L., Koltun, V., Hutter, M.: Learning quadrupedal locomotion over challenging terrain. Sci. Robot. **5**(47), 1–13 (2020)
6. Yin, P., Wang, P., Li, M., Sun, L.: A novel control strategy for quadruped robot walking over irregular terrain. In: IEEE Conference on Robotics. Automation and Mechatronics (RAM), pp. 184–189. IEEE Press, Qingdao (2011)
7. Kim, K.Y., Park, J.H.: Ellipse-based leg-trajectory generation for galloping quadruped robots. J. Mech. Sci. Technol. **22**(11), 2099–2106 (2008)
8. Sakakibara, Y., Kan, K., Hosoda, Y., Hattori, M., Fujie, M.: Foot trajectory for a quadruped walking machine. In: EEE International Workshop on Intelligent Robots and Systems. Towards a New Frontier of Applications, pp. 315–322. IEEE Press, Ibaraki (1990)
9. Rong, X., Li, Y., Ruan, J., Li, B.: Design and simulation for a hydraulic actuated quadruped robot. J. Mech. Sci. Technol. **26**(4), 1171–1177 (2012)
10. Yuan, L., Zhang, Z., Ouyang, R.: Trajectory planning of quadruped robot based on the principle of optimal power. Int. J. Mech. Res. **5**(4), 138–147 (2016)
11. Hyun, D.J., Seok, S., Lee, J., Kim, S.: High speed trot-running: Implementation of a hierarchical controller using proprioceptive impedance control on the MIT Cheetah. Int. J. Rob. Res. **33**(11), 1417–1445 (2014)
12. Semini, C., Tsagarakis, N.G., Guglielmino, E., Focchi, M., Cannella, F., Caldwell, D.G.: Design of HyQ - a hydraulically and electrically actuated quadruped robot. Proc. Inst. Mech. Eng. Part I J. Syst. Control Eng. **225**(6), 831–849 (2011)
13. Li, Y., Li, B., Rong, X., Meng, J.: Mechanical design and gait planning of a hydraulically actuated quadruped bionic robot. J. Shandong Univ. Sci. **41**(5), 32–36 (2011)
14. Wang, L., Wang, J., Wang, S., He, Y.: Strategy of foot trajectory generation for hydraulic quadruped robots gait planning. J. Mech. Eng. **49**(1), 39–44 (2013)
15. Yin, J., Li, H., Dai, Z.: Quadruped robot harmonious control based on RBF-Q learning. Appl. Res. Comput. **30**(8), 2349–2352 (2013)
16. Tuleu, A.: Hardware, software and control design considerations towards low-cost compliant quadruped robots. École Polytechnique Fédérale de Lausanne (2016)
17. Eckert, P., et al.: Towards Rich Motion Skills with the Lightweight Quadruped Robot Serval - A Design, Control and Experimental Study. In: Manoonpong, P., Larsen, J.C., Xiong, X., Hallam, J., Triesch, J. (eds.) SAB 2018. LNCS (LNAI), vol. 10994, pp. 41–55. Springer, Cham (2018). https://doi.org/10.1007/978-3-319-97628-0_4
18. Park, H.W., Kim, S.: Quadrupedal galloping control for a wide range of speed via vertical impulse scaling. Bioinsp. Biomimet. **10**(2), 1–20 (2015)
19. Han, B., Zhu, C., Luo, Q., Zhao, R., Wang, Q.: Key gait parameter optimization for hydraulic quadruped robot. Trans. Beijing Inst. Technol. **38**(10), 1056–1060 (2018)
20. Hildebrand, M.: Further studies on locomotion of the cheetah. J. Mammal. **42**(1), 84–91 (1961)
21. Hildebrand, M., Hurley, J.P.: Energy of the oscillating legs of a fast-moving Cheetah, Pronghorn, Jackrabbit, and Elephant. J. Morphol. **184**, 23–31 (1985)

22. Haberland, M., Karssen, J.G.D., Kim, S., Wisse, M.: The effect of swing leg retraction on running energy efficiency. In: IEEE International Conference on Intelligent Robots & Systems, pp. 3957–3962. IEEE Press, San Francisco (2011)
23. Karssen, J.G.D., Haberland, M., Wisse, M., Kim, S.: The effects of swing-leg retraction on running performance: analysis, simulation, and experiment. Robotica **33**(10), 2137–2155 (2015)
24. Kennedy, J., Eberhart, R.: Particle swarm optimization. Swarm Intell. **1**(1), 33–57 (1995)